Gazi University Journal of Science
GU J Sci
24(4):791-804 (2011)

Damping of Power System Oscillations Using UPFC Based Multipoint Tuning AIPSO-SA Algorithm

Ali AJAMI[1,♠], Hamed ASADZADEH[2]

[1, 2] *Azarbaijan University of Tarbiat Moallem, Electrical Engineering Department, Tabriz, Iran*

Received: 20/02/2011 Revised: 10/06/2011 Accepted:23/06/2011

ABSTRACT

Power system dynamic stability enhancement by unified power flow controller (UPFC)-based stabilizers is thoroughly investigated in this paper. This study presents singular value decomposition (SVD) based approach to assess and measure the controllability of the poorly damped electromechanical modes by different control signals of UPFC. The supplementary controller of UPFC to damping the low frequency oscillation in a weakly connected system is presented. Individual designs of the UPFC controller using adaptive improved particle swarm optimization hybrid with simulated annealing (AIPSO-SA) are discussed. In this paper, the UPFC based controllers' parameters are optimized over a wide range of operating conditions and system parameter uncertainties (multi point tuning) in order to have robust stabilizers. The effectiveness of proposed controller on enhancing dynamic stability is tested through eigen value analysis and time domain simulation. Also nonlinear and electrical simulation results show the validity and effectiveness of the proposed control schemes over a wide range of loading conditions. It is also observed that the proposed UPFC-based damping stabilizers enhance greatly the power system transient stability. Also the simulation results of coordinated design of stabilizer based on δ_{SH} and m_{SE} is presented and discussed.

Key words: Power System Stability, Low Frequency Oscillation Damping, Dynamic Modeling, UPFC, AIPSO-SA

1. INTRODUCTION

Today, power demand grows rapidly and expansion in transmission and generation is restricted with the limited availability of resource and the strict environmental constraints. Consequently, power systems are today much more loaded than before. This causes the power systems to be operated near their stability limits. In addition, interconnection between remotely located power systems gives rise to low frequency oscillations in the range of 0.1-0.3 Hz. If not well damped, these oscillations may keep growing in magnitude until loss of synchronism results [1].

Power system stabilizers (PSSs) have been used in the last few decades to serve the purpose of enhancing power system damping to low frequency oscillations. PSSs, which operate on the excitation system of generators, have proved to be efficient in performing their assigned tasks. However, PSSs may adversely affect on the voltage profile, may result in leading power factor, and may not be able to suppress oscillations caused by large disturbances, especially three phase faults [1].

FACTS devices have shown very promising results when used to improve power system steady-state performance. Through the modulation of bus voltage, phase shift between buses, and transmission line reactance, FACTS devices can cause a substantial increase in power transfer limits during steady-state. Because of the extremely fast control action associated with FACTS-device operations, they have been very promising candidates for utilization in the power system damping enhancement.

Unified power flow controller (UPFC) can be used for power flow control, loop-flow control, load sharing among parallel corridors, enhancement of transient stability, mitigation of system oscillations and voltage (reactive power) regulation [2,3]. Performance analysis and control synthesis of UPFC require its steady-state and dynamic models. A two-source UPFC steady-state model including source impedances is suggested in [4]. Under the assumption that the power system is

♠Corresponding author, e-mail: ajami@azaruniv.edu

symmetrical and operates under three-phase balanced conditions, a steady-state model, a small-signal linearized dynamic model and a state-space large-signal model of a UPFC developed in [5]. In 1999, Wang developed two UPFC models [6, 7] which have been linearized and incorporated into the Phillips-Heffron model. UPFC damping controller design can be found in [1, 8-12]. The supplementary controller can be applied to the shunt inverter through the modulation index of reference voltage signal or to the series inverter through modulation of power reference signal. In [1, 12] the PSO algorithm is used for finding optimum parameters setting of UPFC controllers in order to power system oscillation damping in nominal loading condition.

In this paper, singular value decomposition (SVD) is used to select the control signal which is most suitable for damping the electromechanical (EM) mode oscillations. A single machine infinite bus (SMIB) system equipped with a UPFC controller is used in this study. In This paper the damping controllers design is formulated as an optimization problem to be solved using AIPSO-SA. The aim of the optimization is to search for the optimum controller parameter settings that maximize the minimum damping ratio of the system in single and multi point tuning cases. Eigen value analysis and time domain simulation are used to assess the effectiveness of the proposed controllers to damp low frequency oscillations under different disturbances.

2. MATHEMATICAL MODELLING

Fig. 1 shows a SMIB power system with a UPFC [1]. The four input control signals to the UPFC are m_{SH}, m_{SE}, δ_{SH}, and δ_{SE}. Where, m_{SH} and δ_{SH}, are the modulation index and phase angle of shunt converter output voltage and m_{SE} and δ_{SE} are the modulation index and phase angle of series converter output voltage, respectively. The system data is given in the Appendix A.

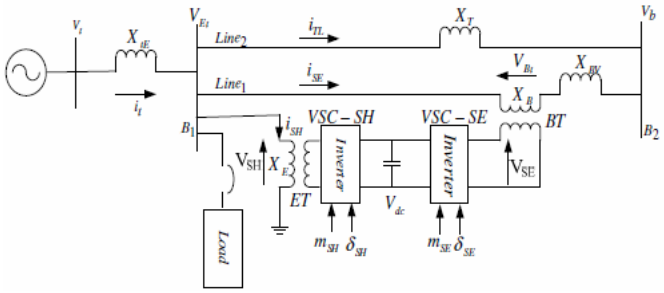

Fig. 1. SMIB power system equipped with UPFC

POWER SYSTEM NON-LINEAR MODEL

The dynamic model of the UPFC is required in order to study the effect of the UPFC for enhancing the small signal stability of the power system. By applying Park's transformation and neglecting the resistance and transients of the exciting transformer (ET) and boosting transformer (BT), the UPFC can be modeled as [1, 4, 6, 12, 13]:

$$V_{SH} = \frac{m_{SH} V_{dc}}{2}\left(\sin\delta_{SH} + j\cos\delta_{SH}\right) \tag{1}$$

$$V_{SE} = \frac{m_{SE} V_{dc}}{2}\left(\sin\delta_{SE} + j\cos\delta_{SE}\right) \tag{2}$$

$$\frac{dV_{dc}}{dt} = \frac{3 m_{SH}}{4 c_{dc}}\left(\sin\delta_{SH}\ i_{SHd} + \cos\delta_{SH}\ i_{SHq}\right) + \frac{3 m_{SE}}{4 c_{dc}}\left(\sin\delta_{SE}\ i_{SEd} + \cos\delta_{SE}\ i_{SEq}\right) \tag{3}$$

Where, V_{Et}, i_{SH}, V_{Bt}, and i_{SE} are the excitation voltage, excitation current, boosting voltage, and boosting current, respectively; C_{dc} and V_{dc} are the DC link capacitance and voltage, respectively. From Fig. 1 we have:

$$\begin{aligned} &\bar{i}_t = \bar{i}_{SE} + \bar{i}_{SH} + \bar{i}_{TL}, \quad \bar{V}_t = j X_{tE} \bar{i}_t + \bar{V}_{Et} \\ &\bar{V}_{Et} = j X_E \bar{i}_{SH} + \bar{V}_{SH}, \quad \bar{V}_{Et} = \bar{V}_{Bt} + j X_{BV} \bar{i}_{SE} + \bar{V}_b \\ &\bar{V}_{Et} = j X_T \bar{i}_{TL} + \bar{V}_b, \qquad \bar{V}_{Bt} = j X_B \bar{i}_{SE} + \bar{V}_{SE} \end{aligned} \tag{4}$$

The relations of excitation and boosting transformers parameters and line 2 currents can be written as:

$$i_{TLd} = \frac{1}{X_T}\left(X_E i_{SHd} + \frac{m_{SH}\sin\delta_{SH} V_{dc}}{2} - V_b \cos\delta \right) \quad (5)$$

$$i_{TLq} = \frac{1}{X_T}\left(X_E i_{SHq} + \frac{m_{SH}\sin\delta_{SH} V_{dc}}{2} - V_b \sin\delta \right) \quad (6)$$

$$i_{SHd} = \frac{X_{BB}}{X_{d2}} E_q^{'} + X_{d7}\frac{m_{SE}\sin\delta_{SE} V_{dc}}{2} + X_{d5} V_b \cos\delta + X_{d6}\frac{m_{SH}\sin\delta_{SH} V_{dc}}{2} \quad (7)$$

$$i_{SHq} = X_{q7}\frac{m_{SE}\cos\delta_{SE} V_{dc}}{2} + X_{q5} V_b \sin\delta + X_{q6}\frac{m_{SH}\cos\delta_{SH} V_{dc}}{2} \quad (8)$$

$$i_{SEd} = \frac{X_E}{X_{d2}} E_q^{'} - \frac{X_{d1}}{X_{d2}}\frac{m_{SE}\sin\delta_{SE} V_{dc}}{2} + X_{d3} V_b \cos\delta + X_{d4}\frac{m_{SH}\sin\delta_{SH} V_{dc}}{2} \quad (9)$$

$$i_{SEq} = \frac{X_{q1}}{X_{q2}}\frac{m_{SE}\cos\delta_{SE} V_{dc}}{2} + X_{q3} V_b \sin\delta + X_{q4}\frac{m_{SE}\cos\delta_{SE} V_{dc}}{2} \quad (10)$$

Where, X_E and X_B are the ET and BT reactance, respectively; the reactance X_{qE}, X_{dE}, X_{BB}, X_{d1}-X_{d7}, and X_{q1}- X_{q7} are given in Appendix B. The non-linear model of the SMIB system of Fig. 1 is:

$$\dot{\delta} = \omega_b(\omega - 1) \quad (11)$$

$$\dot{\omega} = \left(P_m - P_e - D(\omega - 1)\right)/M \quad (12)$$

$$\dot{E}_q^{'} = \left(E_{fd} - \left(x_d - x_d^{'} \right) i_d - E_q^{'} \right)/T_{d0}^{'} \quad (13)$$

$$\dot{E}_{fd} = \left(K_A\left(V_{ref} - v + u_{pss} \right) - E_{fd} \right)/T_A \quad (14)$$

Where, $P_e = V_{td} i_{td} + V_{tq} i_{tq}$, $V_t = \sqrt{V_{td}^2 + V_{tq}^2}$, $V_{td} = x_q i_{tq}$, $V_{tq} = E_q^{'} - x_d^{'} i_{td}$, P_m and P_e are the input and output power, respectively; M and D the inertia constant and damping coefficient, respectively; ω_b the synchronous speed; δ and ω the rotor angle and speed, respectively; $E_q^{'}$, $E_{fd}^{'}$, and V_t the generator internal, field and terminal voltages, respectively; $T_{d0}^{'}$ the open circuit field time constant; x_d, $x_d^{'}$, and x_q the d-axis reactance, d-axis transient reactance, and q-axis reactance, respectively; K_A and T_A the exciter gain and time constant, respectively; V_{ref} the reference voltage; and u_{PSS} the PSS control signal.

POWER SYSTEM LINEARIZED MODEL

The non-linear dynamic equations can be linearized around an operating point condition. The linearized model of power system as shown in Fig. 1 is given as follows:

$$\Delta\dot{\delta} = \omega_b \Delta\omega \quad (15)$$

$$\Delta\dot{\omega} = \frac{1}{M}\left(\Delta P_m - \Delta P_e - D\Delta\omega\right) \quad (16)$$

$$\Delta\dot{E}_q^{'} = \frac{1}{T_{d0}^{'}}\left(-\Delta E_q^{'} + \Delta E_{fd} + (x_d - x_d^{'})\Delta i_{1d} \right) \quad (17)$$

$$\Delta\dot{E}_{fd} = \frac{1}{T_A}\left(-\Delta E_{fd} + K_A(\Delta V_{tref} - \Delta V_t + \Delta u_{pss} \right) \quad (18)$$

$$\Delta\dot{V}_{dc} = K_7\Delta\delta + K_8\Delta E_q^{'} - K_9\Delta V_{dc} + K_{cSH}\Delta m_{SH} + K_{c\delta SH}\Delta\delta_{SH} + K_{cSE}\Delta m_{SE} + K_{c\delta SE}\Delta\delta_{SE} \quad (19)$$

In state-space representation, the power system can be modeled as:

$$\dot{x} = Ax + Bu \quad (20)$$

Where, the state vector x, control vector u, state matrix A and input matrix B are:

$$x = \left[\Delta\delta \;\; \Delta\omega \;\; \Delta E_q' \;\; \Delta E_{fd} \;\; \Delta V_{dc}\right]^T \tag{21}$$

$$u = \left[\Delta u_{pss} \;\; \Delta m_{SH} \;\; \Delta\delta_{SH} \;\; \Delta m_{SE} \;\; \Delta\delta_{SE}\right]^T \tag{22}$$

$$A = \begin{bmatrix} 0 & \omega_b & 0 & 0 & 0 \\ -\frac{K_1}{M} & -\frac{D}{M} & -\frac{K_2}{M} & 0 & -\frac{K_{pd}}{M} \\ -\frac{K_4}{T_{d0}'} & 0 & -\frac{K_3}{T_{d0}'} & \frac{1}{T_{d0}'} & -\frac{K_{qd}}{T_{d0}'} \\ -\frac{K_A K_5}{T_A} & 0 & -\frac{K_A K_6}{T_A} & -\frac{1}{T_A} & -\frac{K_A K_{vd}}{T_A} \\ K_7 & 0 & K_8 & 0 & -K_9 \end{bmatrix} \tag{23}$$

$$B = \begin{bmatrix} 0 & 0 & 0 & 0 & 0 \\ 0 & -\frac{K_{pSH}}{M} & -\frac{K_{p\delta SH}}{M} & -\frac{K_{pSE}}{M} & -\frac{K_{p\delta SE}}{M} \\ 0 & -\frac{K_{qSH}}{T_{d0}'} & -\frac{K_{q\delta SH}}{T_{d0}'} & -\frac{K_{qSE}}{T_{d0}'} & -\frac{K_{q\delta SE}}{T_{d0}'} \\ -\frac{K_A}{T_A} & -\frac{K_A K_{cSH}}{T_A} & -\frac{K_A K_{c\delta SH}}{T_A} & -\frac{K_A K_{cSE}}{T_A} & -\frac{K_A K_{c\delta SE}}{T_A} \\ 0 & K_{cSH} & K_{c\delta SH} & K_{cSE} & K_{c\delta SE} \end{bmatrix} \tag{24}$$

The block diagram of the linearized dynamic model of the SMIB power system with UPFC is shown in Fig. 2 [1]. In addition to the PSS input (u_{PSS}), only one UPFC control input is considered in this Figure.

UPFC CONTROLLERS

The damping controller is designed to produce an electrical torque in phase with the speed deviation according to phase compensation method. The four control parameters of the UPFC (m_{SH}, m_{SE}, δ_{SH} or δ_{SE}) can be modulated in order to produce the damping torque. In order to maintain the power balance between the series and shunt converters, a DC voltage regulator must be incorporated. The DC voltage is controlled through modulating the phase angle of the ET voltage, δ_{SH}. In addition, to dispatch the power flow among transmission lines, a power flow controller is included. The power flow is controlled through modulation the amplitude of the BT voltage, m_{SE}.

In this paper δ_{SH} and m_{SE} are modulated in order to damping controller design. The speed deviation dω is considered as the input to the damping controller. The structure of UPFC based damping controller is shown in Fig. 3 where u can be m_{SH}, m_{SE}, δ_{SH} or δ_{SE}. This controller may be considered as a lead lag compensator. However, an electrical torque in phase with the speed deviation is to be produced in order to improve damping of the system oscillations. The parameters of the damping controller are obtained using AIPSO_SA algorithm.

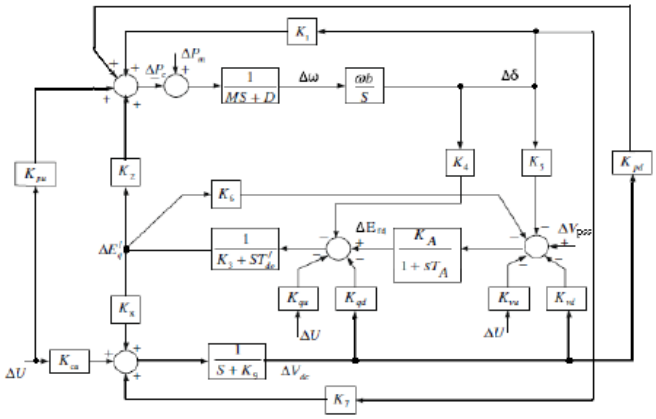

Fig. 2. Modified Heffron–Phillips linearized model [1]

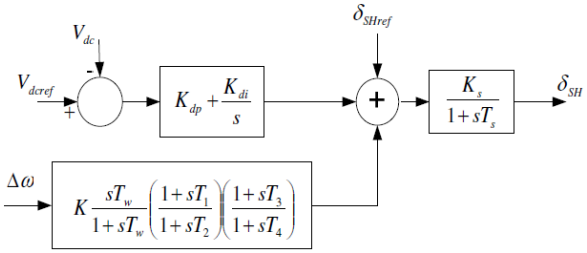

Fig. 3-a. UPFC with lead-lag damping controller and DC voltage regulator.

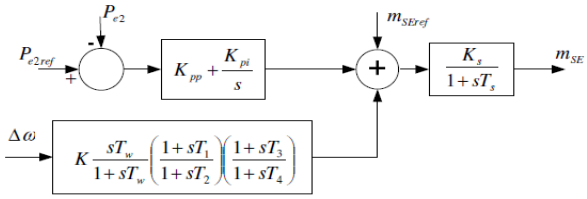

Fig. 3-b. UPFC with lead-lag damping controller and power flow controller.

OBJECTIVE FUNCTION

To select the best stabilizer parameters that enhance most the power system dynamic performance, the problem is formulated so as to optimize a selected objective function J subject to some inequality constraints, which are the maximum and minimum limits of each controller gain K_s and time constants T_1–T_4. In this work,

$$J = min(\xi_i)$$
$$\xi_i = \frac{Real(ith \quad eigenvalue)}{\sqrt{[Real(ith \quad eigenvalue)]^2 + [Im((ith \quad eigenvalue)]^2}} \tag{25}$$

ζ_i = is the damping ratio.

Hence, the design problem can be formulated as maximize J Subject to:

$$K_s^{\min} \le K_s \le K_s^{\max} \qquad T_i^{min} \le T_i \le T_i^{max} \qquad , i = 1,2,3,4$$

$$K_s^{\min} = -100 \qquad K_s^{\max} = 100 \qquad T_i^{\max} = 5 \qquad T_i^{\min} = 0.01$$

The proposed approach employs AIPSO-SA to search for the optimum parameter settings of the given controllers.

3. PROPOSED ALGORITHMS

In recent years, many optimization algorithms are introduced. Some of these algorithms are traditional optimization algorithms. Traditional optimization algorithms use exact methods to find the best solution. The idea is that if a problem can be solved, then the algorithm should find the global best solution. As the search space increases the cost of these algorithms increases. Therefore, when the search space complexity increases the exact algorithms can be slow to find global optimum.

There are several stochastic algorithms. Particle swarm optimization (PSO) and simulated annealing (SA) are two efficient and well known stochastic algorithms.

STANDARD PSO ALGORITHM

The PSO is a population and fitness based algorithm like genetic algorithm. PSO algorithm can be depicted as follow [14-17]:

Suppose that there are m particle in D-dimensional search space. The position of the ith particle is represented as $X_i=[x_{i1}, x_{i2},\ldots, x_{iD}]^T$, and its best position (the position giving the highest fitness value) found so far is recorded and represented as $P_i=[p_{i1}, p_{i2},\ldots, p_{iD}]^T$. The best position found by swarm so far is also recorded and represented as $P_g=[p_{g1}, p_{g2},\ldots, p_{gD}]^T$. During the iteration, the ith particle flies in the search space with the velocity $V_i=[v_{i1}, v_{i2},\ldots, v_{iD}]^T$. Then, the velocity and position of the ith particle update with following equations:

$$v_{id}(t+1) = W * v_{id}(t) + C_1 * rand_1 * (P_{id} - x_{id}(t)) + C_2 * rand_2 * (P_{gd} - x_{id}(t)) \tag{26}$$

$$x_{id}(t+1) = x_{id}(t) + v_{id}(t+1) \tag{27}$$

Where, v_{id} is the velocity of particle ith in dimension dth (is the particle position), W is the inertia weight factor, C_1 and C_2 are two positive constant parameters that are called acceleration coefficients. The $rand_1$ and $rand_2$ are the random functions in the range [0, 1], P_{id} is the best position of the ith particle in dimension dth and P_{gd} is the best position among all particles in the swarm.

IMPROVED PSO ALGORITHM

In PSO algorithm, if the particles converge too quickly, it will result in premature convergence and losing further search ability. Through studying the mechanism of the PSO algorithm, one can conclude that PSO algorithm search optimal solution by tracking two extrema P_i and P_g. so, during the search process, if Pg lies in the local optimum position, all particles will approach P_g very quickly. This will result in premature convergence. In order to solve this question, during the iteration, it must be avoided that P_g falls into local optimum position. In this paper, the scheme of selecting P_g is improved. During the iteration of IPSO algorithm, we don't simply select the particle with the highest fitness as P_g, but select a particle from several particles with the highest fitness using roulette wheel method. Concretely, let the positions of the first L particle with highest fitness in particle swarm be P_g^1, P_g^2, … , P_g^L and their fitness be g^1 , g^2 , … , g^L . According to roulette wheel selection method, the probability of P_g^i (i=1,2, … , L) that is selected as P_g is given in (28) [18, 19].

Thus, the IPSO algorithm maintains the character of the basic algorithm. Also the IPSO algorithm searches optimal solution by tracking two extrema. However, when the best particle found by the swarm falls into local minima, other different particles maybe selected as P_g, and the particles will fly to other direction. Then, it is avoided that all particles approach the local optima very quickly, and the probability of premature converging to local optima is decreased. Although the selected particle is not the optimal particle, it is a suboptimal particle. This ensures that the particle swarm flies to a good direction. In IPSO algorithm, L is a very important value. If is too small, the roulette wheel selection method will have very little effect on this algorithm. On the other hand, if L is too large, the particle selected as P_g is perhaps a bad particle. This will affect the search ability of IPSO. In application, L is set as [m/10], where [x] means the largest integer do not exceed x.

AIPSO-SA ALGORITHM

Simulated Annealing (Metropolis et al. 1956, Kirkpatrick et al. 1983) [20] is a metastrategy local search method that attempts to avoid producing the poor local maximum inherent in the steepest ascent method. The main idea behind Simulated Annealing is an analogy with the way in which liquids freeze and crystallize. The simulated annealing algorithm aims to achieve a global optimum by slowly converging to a final solution, making downwards moves with occasional "upwards" moves (the probability of these occurring decreasing with the "temperature") and thus hopefully ending up in a global optimum. The most significant character of SA is the probabilistic jumping property, i.e. a worse solution has a probability to be accepted as the new solution. Moreover, by adjusting the temperature, such a jumping probability can be controlled.

Slow convergence of PSO before providing an accurate solution is a drawback, closely related to its lack of any adaptive accelerators in the velocity updating formulae. In (27), C_1 and C_2 determine the step size of the particles movements through the P_{id} and P_{gd}, respectively. In the original PSO, these step sizes are constant and for the all particles are same. For doing more sensitive and faster movements, new step sizes can be modified, which they should accelerate the convergence rate. In each iteration, the value of objective function is a criterion that presents the relative improvement of this movement in respect to the previous iteration movement. Thus the difference between the values of objective function in the different iterations can select as the accelerators. Adding two additional coefficients to the original step sizes in (27), it causes to adaptive movements. Therefore, velocity updating formula can be obtained from (29).

$$O^i = g^i \Big/ \sum_{j=1}^{L} g^j \qquad (i = 1,2,...,L) \tag{28}$$

$$\begin{aligned} v_{id}(t+1) = {} & W * v_{id}(t) + \\ & C_1 * rand_1 * \left(f(P_{id}(t))\right) - f(x_{id}(t)) * (P_{id} - x_{id}(t)) + \\ & C_2 * rand_2 * \left(f(P_{gd}(t))\right) - f(x_{id}(t)) * (P_{gd} - x_{id}(t)) \end{aligned} \tag{29}$$

Where, f (P_{id}(t)) is the best fitness function that is found by ith particle and f (P_{gd}(t)) is the best fitness function that is found by swarm up to now. Globally optimize an objective function in a given search domain consists in finding its global optimum without being trapped in any local optimum. When strongly multi-modal problems are being optimized, PSO algorithm usually suffers from the premature suboptimal convergence (simply premature convergence or stagnation) which occurs when some poor particles attract the swarm, due to a local optimum or bad initialization, preventing further exploration of the search space. According to [19], although PSO finds good solutions much faster than other evolutionary algorithms, it usually can not improve the quality of the solutions as the number of iterations is increased. The rational behind this problem is that particles converge to a single point, which is on the line between the global best and personal best positions. This point is not guaranteed to be even a local optimum. Another reason for this problem is the fast rate of information flow between particles, resulting in the creation of similar particles (with a loss in diversity) which increases the possibility of being trapped in local minima [20]. This feature prevents standard PSO from

being really of practical interest for a lot of applications. By combining AIPSO with SA algorithm, we can get a new hybrid optimization approach, called AIPSO-SA [21]. Using of jumping property of SA can help to more diversification that it guarantees the algorithm escapes from local optimum. As mentioned in section 4.2. SA accepts worse solutions with a probability of exp(−Δ/T). When algorithm becomes trapped in a local optimum valley it can jump of valley with a probability leaded to more diversity. In fact, AIPSO-SA has rapid convergence but not premature convergence. In AIPSO-SA algorithm, we name every point which is found by equation (30), the temporary point $x_{id}(p)$ ($x_{id}(p) = x_{id}(t+1)$). If $x_{id}(p)$ is better than $x_{id}(t)$, it will be accepted and if it is worse than $x_{id}(t)$, we will accept it with probability of exp(−Δ/T) , (Δ=f(x_{id}(p))-f(x_{id}(t))). This process is performed for all particles. When a temporary point rejected, that we name it a detoured particle $x_{id}(d)$, it is given back in the opposite direction of the previous movement. These descriptions are formulated by the following equations.

$$\begin{aligned} &x_{id}(p) = x_{id}(t) + v_{id}(t) \\ &\Delta = f(x_{id}(p)) - f(x_{id}(t)) \\ &If \quad \Delta \prec 0 \quad then \quad \begin{cases} x_{id}(t+1) = x_{id}(p) \end{cases} \\ &If \quad \Delta \geq 0 \quad then \quad \begin{cases} x_{id}(d) = x_{id}(p) + \alpha * v_{id}(t) \\ x_{id}(t+1) = x_{id}(d) \end{cases} \end{aligned} \tag{30}$$

Where,

$$\alpha = \begin{cases} +1 & probability = e^{(-\Delta/T)} \\ -1 & other\ wise \end{cases} \tag{31}$$

Increasing the value of the inertia weight, W, will increase the speed of the particles resulting in more exploration (global search) and less exploitation (local search). On the other hand, decreasing the value of W will decrease the speed of the particle resulting in more exploitation and less exploration. Thus, an iteration-dependent weight factor often outperforms a fixed factor. The most common functional form for this weight factor is linear, and changes with step i as follows:

$$W = W_{max} - \frac{W_{max} - W_{min}}{N_{iter}} \times iter \tag{32}$$

Where, N_{iter} is the maximum number of iterations (N_{iter}=100), iter is number of iteration (iter=1, 2,..., N_{iter}) and W_{max} and W_{min} are selected to be 0.9 and 0.1, respectively.

4. SIMULATION RESULT

In this section the simulation results of linearized model and non linear electrical model are presented.

CONTROLLABILITY MEASURE

The numerical values of matrices A and B are achieved by equations 23 and 24 are given in appendix C. To measure the controllability of the EM mode by a given input (control signal), the singular value decomposition (SVD) is employed [1]. The minimum singular value, σ_{min}, of the matrix [λI–A b_i] indicates the capability of the ith input to control the associated mode with the eigen value λ. Where b_i is a column vector corresponding to the ith input. Actually, the higher σ_{min}, is concerned to the higher controllability of this mode by the considered input. Also, the controllability of the EM mode can be examined with all inputs (δ_{SH}, δ_{SE}, m_{SH} and m_{SE}) in order to identify the most effective one to control the mode. The minimum singular value, σ_{min}, is estimated over a wide range of operating conditions. For SVD analysis, P_e ranges from 0.05 to 1.4 pu and Qe = [-0.15, 0, 0.15]. At each loading condition, the system model is linearized, the EM mode is identified, and the SVD-based controllability measure is implemented. For comparison purposes, the minimum singular value for all inputs at Qe = -0.15, 0.0 and 0.15 pu is shown in Figs. 4-a, b and c, respectively. From these figures, the following can be noticed:

- EM mode controllability via δ_{SH} is always higher than other inputs.
- It can be seen that the controllability of the electromechanical mode with all inputs increases with loading at lagging, leading and unity power factor.
- All control signals except δ_{SH} suffer from low controllability to EM mode at low loading conditions.

APPLICATION OF PROPOSED ALGORITHMS TO DESIGN PROCESS

The PSO, IPSO, AIPSO-SA algorithm has been applied to search for the optimal parameter settings of all supplementary controllers so that the objective function is optimized. To assess the effectiveness of the proposed controllers, four different loading conditions are considered for eigen value analysis. These conditions are:

1. Nominal loading (Pe, Qe) = (1.0, 0.015) pu.
2. Light loading (Pe, Qe) = (0.3, 0.015) pu.
3. Heavy loading (Pe, Qe) = (1.1, 0.40) pu.
4. Leading power factor loading (Pe, Qe) = (1.1, 0.40) pu.

SINGLE POINT TUNING

1. STABILIZER DESIGN

In this section, the stabilizers are tuned with only the nominal loading condition. The final parameter settings of the supplementary controllers are given in Table 1. The convergence rates of the objective function for PSO, IPSO, AIPSO-SA algorithms are shown in Fig. 5. It is clear that the δ_{SH}-based controller improves greatly the system damping compared to other controllers.

2. EIGEN VALUE ANALYSIS

The system electromechanical mode eigen value and its damping ratio(ζ) with and without the proposed UPFC stabilizer inputs are given in Table 2 for nominal, light, heavy and leading power factor loading conditions, respectively. It is clear that the proposed stabilizers greatly improve the system stability. It is also clear that the m_{SH}, δ_{SE}-based stabilizer have relatively poor capabilities to enhance the EM mode damping when the system operates at light, heavy and leading power factor loading conditions and m_{SE}-based stabilizer have relatively poor capabilities to enhance the EM mode damping when the system operates at leading power factor loading condition.

MULTIPLE POINT TUNING

In this section, the UPFC-based controllers' parameters are optimized over a wide range of operating conditions and system parameter uncertainties in order to have robust stabilizers. Four loading conditions represent nominal, light, heavy, and leading power factor are considered. Each loading condition is considered without and with parameter uncertainties as given in Table 3. Each loading condition is considered in 1- without uncertainties, 2- 30% increase and 3- 30% decrease of line reactance, 4- 25% increase and 5- 25% decrease of machine inertia 6- 30% increase and 7- 30% decrease of field time constant T'_{d0}. Hence, the total number of points which considered for design process is 28.

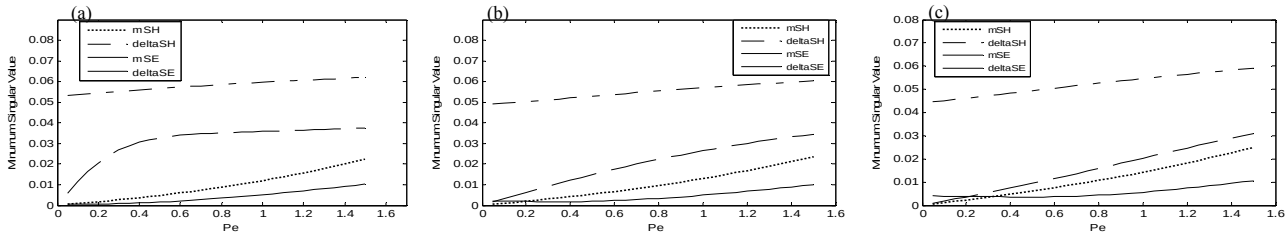

Fig. 4. Minimum singular value with all stabilizers at a) Qe = 0.15 b) Qe = 0.0 c) Qe =- 0.15

Table 1. The optimal settings of the individual controller

	PSO				IPSO				AIPSO-SA			
	m_{SE}	m_{SH}	δ_{SE}	δ_{SH}	m_{SE}	m_{SH}	δ_{SE}	δ_{SH}	m_{SE}	m_{SH}	δ_{SE}	δ_{SH}
Ks	-55.2079	-38.25	99.3072	-47.24	-100.0	-81.24	100.0000	-61.45	-50.10	-19.07	100.0000	-93.42
T_1	5.0000	1.2717	3.4107	1.0083	3.7329	1.2100	3.3041	2.1044	3.7704	2.4068	3.9761	1.0171
T_2	4.5692	3.1702	1.9179	2.0794	0.4728	0.0010	0.1718	1.2936	0.6363	0.0010	0.2818	3.4153
T_3	4.6494	0.3506	3.2665	3.4604	1.1912	0.2323	4.9425	0.9452	4.0309	0.1547	2.8015	4.1950
T_4	0.5100	0.0010	0.1270	2.1989	2.3188	4.9999	2.8054	2.4339	3.6947	2.1500	1.6396	4.1950

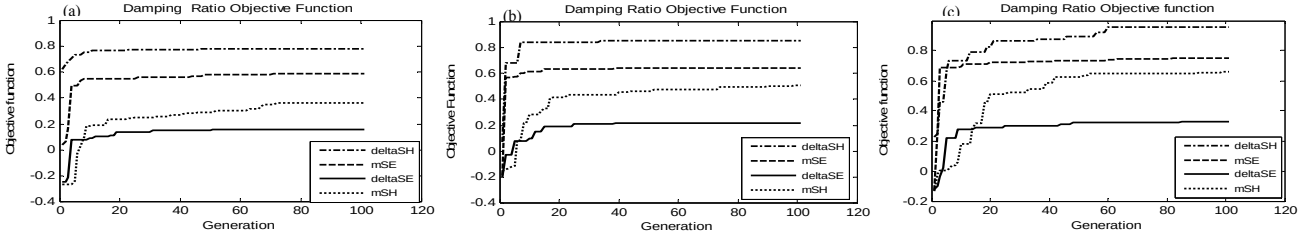

Fig. 5. Objective function in single point tuning case of δSH, δSE, mSH and mSE-based stabilizers, a) PSO b) IPSO c) IPSO-SA algorithm

1. STABILIZER DESIGN

The convergence rate of the objective function in multi point tuning case when δ_{SH}, δ_{SE}, m_{SH} and m_{SE}-based stabilizers are design individually is shown in Fig. 6. The final setting of the optimize parameters for the proposed stabilizers are given in Table 4.

2. EIGEN VALUE ANALYSIS

The system electromechanical mode eigen value and its damping ratio without and with the proposed stabilizers at nominal, light, heavy and leading power factor loading conditions are given in Table 5. It is clear that the proposed robust stabilizers are effective at all points considered. However, the values of ζ corresponding to the EM mode resulting from using δ_{SH} and m_{SE} as control signals are much higher than those resulting from using m_{SH} and δ_{SE}. This agrees with the SVD analysis carried out previously.

3. NON-LINEAR TIME SIMULATION

The system behavior due to the utilization of the proposed controllers under transient conditions has been tested by applying three large disturbances: 1) a 3-phase fault with 6-cycle duration is occurred at t =10 sec at the middle of Line 1 for all loading conditions, 2) a 3-phase

fault with 6-cycle duration occurred at t =10 sec at infinite bus for nominal loading condition, 3) connection a large load (P=400 MW, Q=400 MVA) in bus B1 at t=15sec. The system response is shown in figures 7, 8. The Fig. 7 represents deviation in rotor speed, load angle, generator output active power and power flow of line 1 when the damping controller is not installed. Rotor speed deviations are shown in Fig.8 (a-d) for different loading condition when a three phase fault is accrued at middle of line 1. Also the load angle variations are presented in Fig.8 (e-h) in this case. The variations of generator output power are shown in Fig.8 (i-l). Figures 9 and 10 present the non linear simulation results when a three phase fault is occurred at infinite bus and a large load is connected to bus B1, respectively. It can be seen that δ_{SH}-based stabilizer provide an excellent damping characteristics and enhance the first swing stability at all loading conditions.

Table 2. Eigenvalues For Δsh, Δse, Msh And Mse Based Stabilizers (PSO, IPSO, AIPSO-SA)

		Nominal	Light	Heavy	Leading power factor
System without UPFC		0.7669 ± 3.5160i ζ=-0.2131	0.2687 ± 3.0104i ζ=-0.0889	0.6934 ± 3.4953i ζ=-0.1945	0.7238 ± 3.2797i ζ= -0.2155
PSO	δ_{SH}	-9.9266 ± 7.8959i ζ= 0.7826	-0.4032 ±0.4236i ζ= 0.6894	-0.5321±0.4212i ζ= 0.7832	-0.8313±1.5441i ζ= 0.4741
	m_{SH}	-1.90 ± 4.80i ζ= 0.3646	-0.40 ± 3.20i ζ= 0.1258	-0.20 ± 4.80i ζ= 0.0371	-0.0008 ± 0.0028i ζ= 0.2789
	δ_{SE}	-0.6460 ± 4.0714i ζ= 0.1563	0.2696 ± 3.1557i ζ= -0.0851	1.0439 ± 4.5384i Z= -0.2242	0.0242 ± 2.5657i ζ= -0.0094
	m_{SE}	-1.2546 ± 1.7209i ζ= 0.5891	-0.5465 ± 1.3516i ζ= 0.3749	-2.2025 ± 4.2479i ζ= 0.4603	0.3372 ± 2.3176i ζ= -0.1440
IPSO	δ_{SH}	-1.2570 ± 0.5930i ζ= 0.8579	-0.4342 ± 0.4114i ζ= 0.7259	-0.6138 ± 0.4263i ζ= 0.8213	-0.6537 ± 1.4817i ζ= 0.4037
	m_{SH}	-2.50 ± 4.30i ζ= 0.5082	-0.5 ± 3.2i ζ= 0.1481	-0.90 ± 4.90i ζ= 0.1857	0.1593 ± 2.7275i ζ= 0.0583
	δ_{SE}	-0.9081 ± 4.0596i ζ= 0.2183	0.2943 ± 3.1707i ζ= -0.0924	0.7332 ± 4.5754i Z= -0.1582	-1.50 ± 2.80i ζ= 0.4668
	m_{SE}	-1.8960 ± 2.2306i ζ= 0.6476	-0.8819 ± 1.5957i ζ= 0.4837	-2.6407 ± 4.5727i ζ= 0.5001	-0.1238 ± 2.5988i ζ= 0.0476
AIPSO-SA	δ_{SH}	-1.1611 ± 0.1389i ζ= 0.9559	-0.2698 ± 0.3684i ζ= 0.5909	-0.4124 ± 0.3724i ζ= 0.7422	-0.6537 ± 1.4817i ζ= 0.4037
	m_{SH}	-3.00 ± 3.40i ζ= 0.6582	-0.490 ± 3.020i ζ= 0.1598	-1.40 ± 4.30i ζ= 0.3062	0.1593 ± 2.7275i ζ= 0.0583
	δ_{SE}	-1.3787 ± 3.9810i ζ= 0.3265	-0.490 ± 3.020i ζ= 0.1598	0.3062 ± 4.5698i Z= -0.0669	-1.50 ± 2.80i ζ= 0.4668
	m_{SE}	-2.3806 ± 2.0865i ζ= 0.7512	-0.8940 ± 1.6395i ζ= 0.4787	-1.5772 ± 1.6101i ζ= 0.4471	-0.1238 ± 2.5988i ζ= 0.0476

Table 3. Loading conditions and parameter uncertainties

Loading	(P, Q) pu	Condition Parameter uncertainties
Nominal	(1, 0.015)	No parameter uncertainties
Light	(0.3, 0.015)	30% increase and decrease of line reactance X
Heavy	(1.1, 0.4)	25% increase and decrease of machine inertia M
Leading P.F.	(0.7, -0.3)	30% increase and decrease of field time constant T'_{d0}

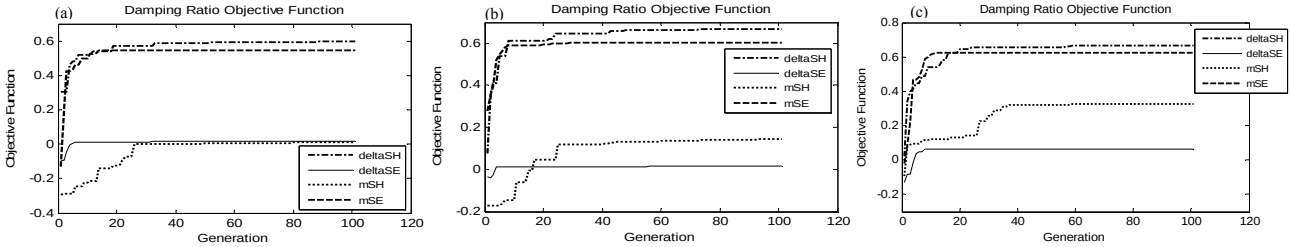

Fig. 6. Objective function in multi point tuning case of δ_{SH}, δ_{SE}, m_{SH} and m_{SE}-based stabilizers, a) PSO b) IPSO c) IPSO-SA algorithm

Table 4. The optimal settings of the individual controller in the multi point tuning case

	PSO				IPSO				AIPSO-SA			
	m_{SE}	m_{SH}	δ_{SE}	δ_{SH}	m_{SE}	m_{SH}	δ_{SE}	δ_{SH}	m_{SE}	m_{SH}	δ_{SE}	δ_{SH}
K_S	100.00	-13.09	-100.00	-100.00	100.00	-9.727	-52.73	-100.00	-100.00	-80.9019	-57.6390	100.0000
T_1	5.0000	0.4045	2.9597	0.8936	5.0000	0.2260	5.0000	0.7338	3.6733	5.0000	3.2735	5.0000
T_2	1.8880	0.0010	0.7469	2.0305	2.4039	1.5550	0.8953	4.9916	1.5262	1.7377	4.4766	2.2018
T_3	5.0000	3.9733	3.4684	1.1362	5.0000	3.5024	4.5373	3.6700	0.7456	5.0000	0.1301	5.0000
T_4	2.1646	4.2177	3.5679	1.3958	2.4096	0.0010	3.5085	1.4830	4.9333	2.0592	0.0010	2.2019

COORDINATED DESIGN OF δ_{SH}, m_{SE} BASED CONTROLLER

In this section coordinated design of two stabilizers based on δ_{SH} and m_{SE} is investigated. With applying the AIPSO-SA algorithm in the multi point tuning case the controller parameters based δ_{SH} and m_{SE} is obtained. The final setting of the optimize parameters for the proposed stabilizer are given in Table 6. The convergence rate of the objective function in this case when δ_{SH} and m_{SE} based stabilizers are designed coordinately is shown in Fig. 11.

The system electromechanical mode eigen value and its damping ratio in the coordinated design of stabilizers at deferent loading conditions are given in Table 7.

With comparing the results of this method and individual design of stabilizer, it is seen that in coordinated design the damping ratio of deferent loading conditions is increased.

Simulation results of coordinated design are presented in Fig. 12. This figure shows variations of rotor speed, load angle, generator output active power and active power flow of line 1 in the nominal loading when a 5% step changing in the mechanical input power of generator (Pm) is occurred. From this figure it can be obtained that the coordinated designed controller has good performance and fast response in damping of low frequency oscillations caused by step changing in the mechanical input power of generator.

Table 5. System eigen values for δ_{SH}, δ_{SE}, m_{SH} and m_{SE} based stabilizers in multi point tuning case (by PSO, IPSO, AIPSO-SA)

		Nominal	Light	Heavy	Leading power factor
System without UPFC		0.9096 ± 3.2766i Z= -0.2675	0.2670 ± 2.9444i Z= -0.0903	0.8354 ± 3.2629i ζ= -0.2480	0.8269 ± 3.0908i ζ= -0.2584
PSO	δ_{SH}	-2.1826 ± 2.2757i Z= 0.6922	-0.2659 ± 0.3307i Z= 0.6266	-2.5404 ± 2.4680i ζ= 0.7173	-1.3854 ± 1.3439i ζ= 0.7178
	m_{SH}	-0.70 ± 3.20i Z= 0.2015	-0.40 ± 3.20i Z= 0.1219	-0.70 ± 4.10i ζ= 0.1700	-0.30 ± 2.60i ζ= 0.1058
	δ_{SE}	-1.2398 ± 6.4894i Z= 0.1877	-0.1076 ± 2.9854i Z= 0.0360	-0.7034 ± 5.9953i ζ= 0.1165	-0.2659 ± 2.1849i ζ= 0.1208
	m_{SE}	-0.5959 ± 0.7773i Z= 0.6084	-0.5672 ± 0.7533i Z= 0.6015	-0.5321 ± 0.7089i ζ= 0.6003	-0.6612 ± 0.9207i ζ= 0.5833
IPSO	δ_{SH}	-2.3838 ± 2.1191i Z= 0.7474	-0.3346 ± 0.3432i Z= 0.6981	-0.4460 ± 0.3797i ζ= 0.7614	-9.6190 ± 6.7565i ζ= 0.8183
	m_{SH}	-3.20 ± 6.90i Z= 0.4168	-0.60 ± 2.90i Z= 0.1934	-2.90 ± 6.10i ζ= 0.4224	-0.60 ± 2.10i ζ= 0.2637
	δ_{SE}	-1.2424 ± 6.4692i Z= 0.1886	-0.1100 ± 2.9836i Z= 0.0369	-0.7055 ± 5.9804i ζ= 0.1172	-0.2529 ± 2.1628i ζ= 0.1162
	m_{SE}	-10.2708 ± 10.7709i Z= 0.6901	-10.2484 ± 7.9618i Z= 0.7897	-10.2470 ± 10.7863i ζ= 0.6888	-1.1787 ± 1.1985i ζ= 0.7012
AIPSO-SA	δ_{SH}	-2.3730 ± 2.1124i Z= 0.7469	-0.3311 ± 0.3402i Z= 0.6974	-0.4419 ± 0.3745i ζ= 0.7629	-9.6218 ± 6.7589i ζ= 0.8183
	m_{SH}	-4.530 ± 9.580i Z= 0.4273	-1.120 ± 2.660i Z= 0.3871	-0.0428 ± 0.0893i ζ= 0.4318	-0.660 ± 1.270i ζ= 0.4600
	δ_{SE}	-1.6097 ± 8.0558i Z= 0.1959	-0.2728 ± 2.9730i Z= 0.0914	-1.1788 ± 7.3010i ζ= 0.1594	-0.2430 ± 1.7861i ζ= 0.1348
	m_{SE}	-0.7793 ±0.7184i Z= 0.7353	-0.7196 ± 0.6505i Z= 0.7418	-0.6628 ± 0.6369i ζ= 0.7211	-0.8826 ± 0.9682i ζ= 0.6737

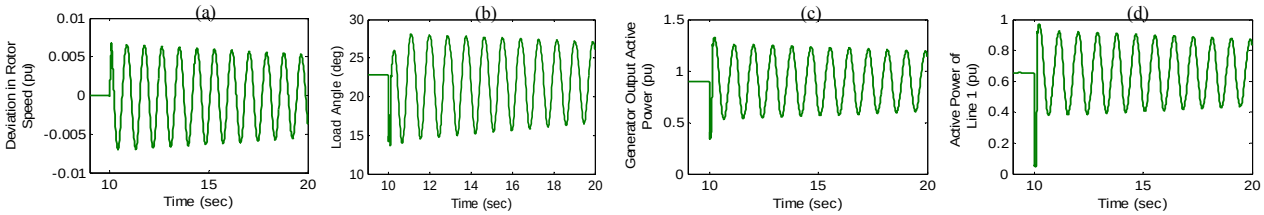

Fig 7. System response for a 6-cycle fault at middle of line 1 (Without damping controller)
a) Deviation in rotor speed (pu) b) Load angle (deg) c) Generator out put active power d) Active power of line 1 (pu)

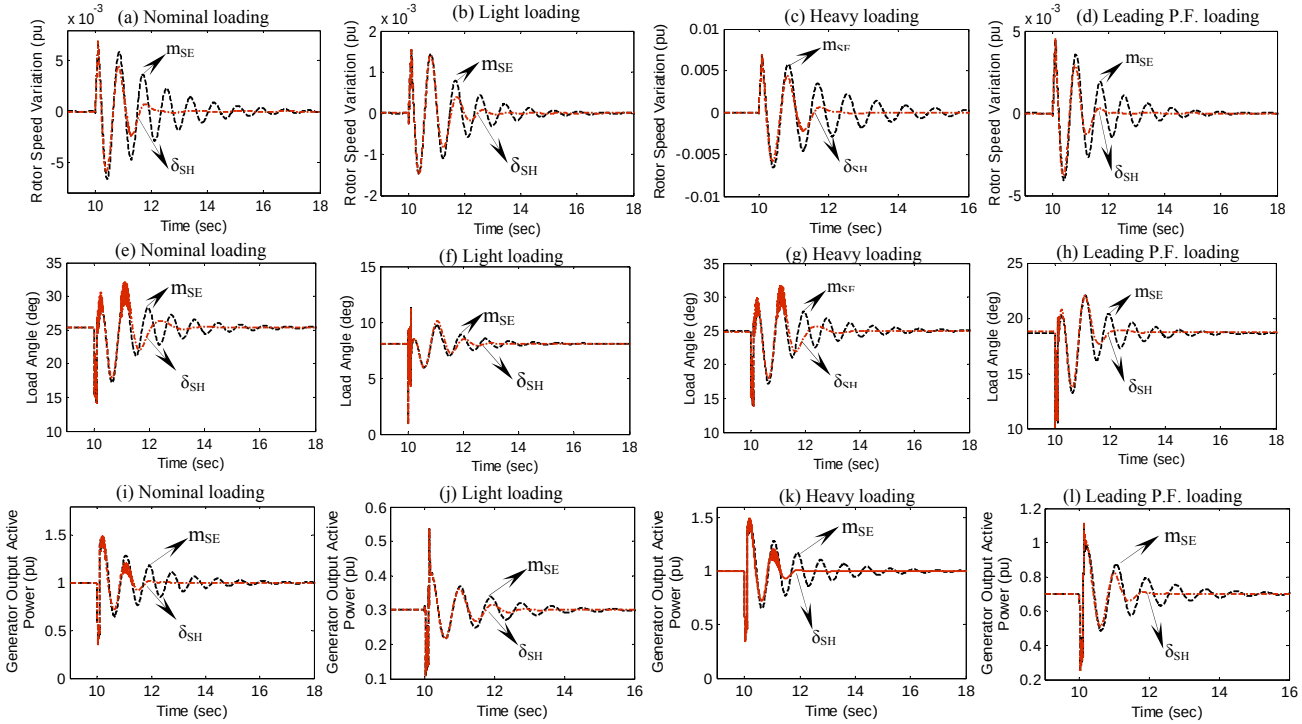

Fig 8. System response for a 6-cycle fault at middle of line 1 for different loading conditions when damping controller is installed.

Table 6. The optimal settings of coordinated controller in the multi point tuning case using AIPSO-SA

	δ_{SH}	m_{SE}
Ks	-100.0000	100.00
T1	0.1683	5.0000
T2	0.0010	1.6939
T3	0.2713	5.0000
T4	3.9661	4.0368

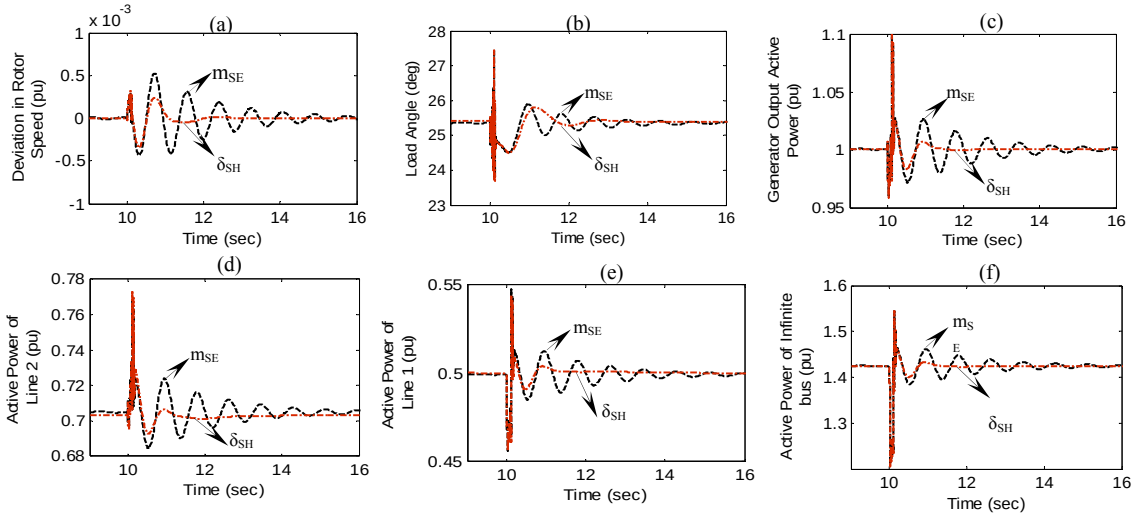

Fig 9. System response for a 6-cycle fault at infinite bus in nominal Loading

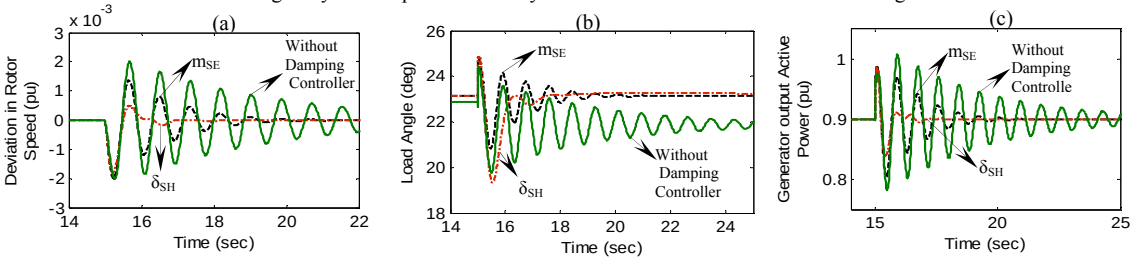

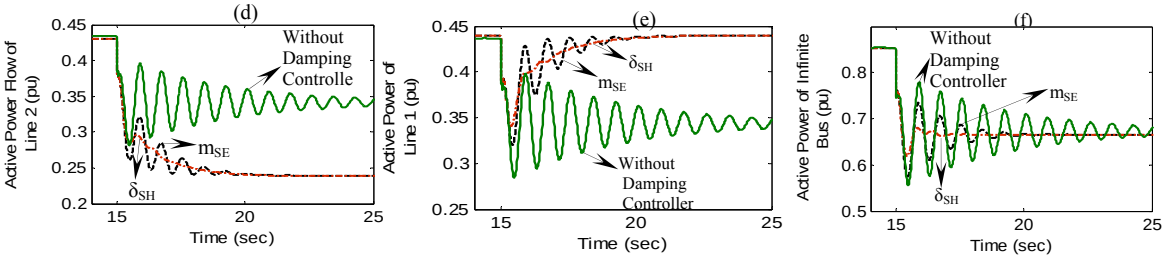

Fig 10. System response for a large load connecting at bus 1

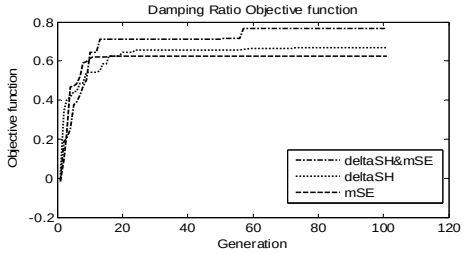

Fig. 11. Variation of the objective function in multi point tuning case and coordinated design using IPSO-SA algorithm

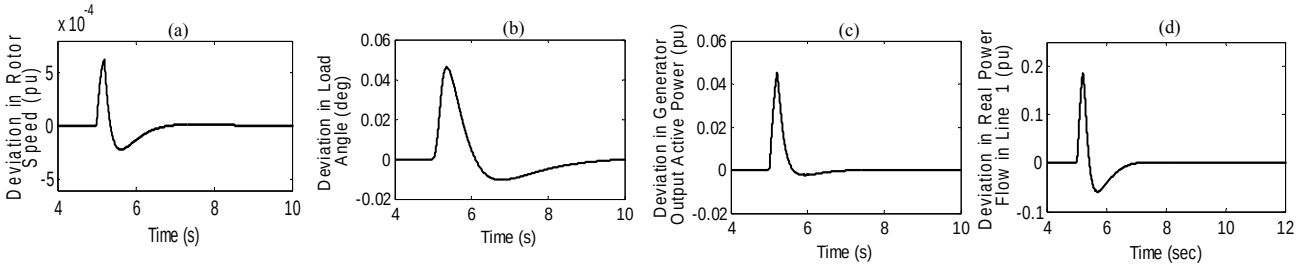

Fig. 12. System response to 5% step changing in Pm using multi point tuning case and coordinated design based AIPSO-SA
a) Rotor speed b)Load angle c)Generator output active power d)Active power flow of line 1

Table 7. The system electromechanical mode eigen value and its damping ratio in the coordinated design of stabilizers based aipso-sa

	Nominal	Light	Heavy	Leading power factor
System without UPFC	0.9096 ± 3.2766i Z= -0.2675	0.2670 ± 2.9444i ζ= -0.0903	0.8354 ± 3.2629i ζ= -0.2480	0.8269 ± 3.0908i ζ= -0.2584
With UPFC Based AIPSO-SA	-0.970 ± 0.590i ζ= 0.8547	-0.510 ± 0.310i ζ= 0.8547	-0.260 ± 0.210i ζ= 0.7831	-0.690 ± 0.470i ζ= 0.8243

2. CONCLUSION

In this paper, SVD has been employed to evaluate the EM mode controllability to four UPFC control signals. It has been shown that the EM mode is most strongly controlled via δ_{SH} for a wide range of loading conditions. In addition, SVD analysis has illustrated that the EM mode is poorly controlled through m_{SH} and δ_{SE}. The AIPSO-SA optimization technique has been proposed to design the UPFC controllers individually and δ_{SH}, m_{SE} coordinately. PSO, IPSO and AIPSO-SA have been utilized to search for the optimal controller parameter settings that optimize a damping ratio based objective function. The presented simulation results show the robustness of designed controllers vice versa variation of operating conditions and system parameters uncertainties (multi point tuning). The presented results show clearly the superiority of the δ_{SH}-based stabilizer and proposed coordinated design approach in enhancing the low frequency oscillations damping. Also simulation results through non-linear power system model have proved the conclusions drawn from SVD analysis and show the effectiveness of proposed controller on enhancing dynamic stability.

REFERENCES

[1] T. Al-Awami A., Magid A., M., Abido A., "A Partical Swarm Based Approach of Power System Stability Enhancement With Unified Power Flow Controller", ***Electrical Power and Energy System***, 29:251-259 (2007).

[2] Gyugyi L., Schauder C.D., Williams S.L., Rietman T.R., Torgerson D.R., Edris A., "The Unified Power Flow Controller: A New Approach to Power Transmission Control", ***IEEE Trans. on Power Delivery***, , 10(2):1085-1097 (1995).

[3] Gyugy L., "A Unified Power Flow Control Concept for Flexible AC Transmission Systems", ***IEE Proc Gen Trans Distrib***, 139(4):323-333 (1992).

[4] Nabavi-Niaki A., Iravani M.R., "Steady-state and dynamic models of unified power flow controller (UPFC) for power system studies", ***IEEE Transactions on Power System***, 11(4):1937–1943 (1996)

[5] Stefanov P.C, Stankovic A.M., "Modeling of UPFC operation under unbalanced conditions with

dynamic phasors", ***IEEE Transactions on Power System***, 17(2): 395–403 (2002).
[6] Wang H.F, "Damping function of unified power flow controller", ***IEE Proc Gen Trans Distrib***, 146(1): 81–87 (1999).
[7] Wang H. F., "Application of modeling UPFC into multi-machine power systems", ***IEE Proc Generation Transmission Distribution***, 146(3): 306–312 (1999).
[8] Padiyar, K.R., Kulkarni, A.M., "Control Design and Simulation of Unified Power Flow Controller", ***IEEE Transactions on Power Delivery***, 13(4): 1348-1354 (1997).
[9] Uzunovic, E., Canizares, C.A., Reeve, J., "EMTP Studies of UPFC Power Oscillation Damping", ***Proceedings of the North American Power Symposium (NAPS)***, San Luis Obispo, CA, October, p. 405-410 (1999).
[10] Mithulananthan N., Canizares C., Roeeve J., Rogers G., "Comparison of PSS, SVC, and STATCOM for Damping Power System Oscillations", ***IEEE Trans. On Power Systems***, 18(2) (2003).
[11] Pandey R. K.,. Singh N. K, "Minimum Singular Value Based Identification of UPFC Control Parameters", TENCON 2006, ***IEEE Region 10 Conference***, November, p. 1-4 (2006).
[12] Shayeghi H., Shayanfar H. A., Jalilzadeh S., Safari A., "A PSO Based Unified Power Flow Controller for Damping of Power System Oscillations", ***Energy conversion and management***, 50: 2583-2592 (2009).
[13] Schauder, C., Metha, H., "Vector Analysis and Control of Advanced Static VAR Compensators", ***IEE Proceedings-C***, 140(4): 299-306 (1993).
[14] Kennedy J, Eberhart R., "Particle swarm optimization", ***Proc IEEE Int Conf Neural Networks***, , 4: 1942–1948 (1995).
[15] Eberhart R, Kennedy J., "A new optimizer using particle swarm theory, ***In Proc Sixth Int Symp Micro Machine Human Science***, 4–6 October, p. 39–43 (1995).
[16] Riget J., Vesterstrom J., "A Diversity-Guided Particle Swarm Optimizer-The ARPSO", ***EVALife Technical Report***, no 2002-2, (2002).
[17] Kennedy J., Eberhart R., Shi Y., "Swarm intelligence", ***Morgan Kaufmann Publishers***, San Francisco, (2001).
[18] Yong-gang L., Wei-hua G., Chun-hua Y., Jie L., "Improved PSO algorithm and its application", ***Journal of central south university of technology***, October, 12: 222-226 (2005).
[19] Angleine P., "Using Selection to Improve Particle Swarm Optimization", ***In Optimization Conference on Evolutionary Computation***, Piscataway, New Jersey, USA, IEEE service center, , p. 84-89 (1998).
[20] Kirkpatrick, S., Gelatt, C.D., Vecchi, "Optimization by Simulated Annealing", ***In Science,*** 220: 671-680 (1983).
[21] Ajami A., Asadzadeh H., "AIPSO-SA Based Approach for Power System Oscillation Damping With STATCOM", ***Journal of International Review on Electrical Engineering***, No. 4, June, (2010).

APPENDIX A

The test system parameters are:

Machine: $x_d = 1$; $x_q = 0.6$; $x'_d = 0.3$; D = 0; M = 8.0; $T'_{d0} = 5.044$; v = 1.05; ; f = 60 Hz

Exciter: $K_A = 50$; $T_A = 0.05$; $E_{fd}\_max = 7.3$; $E_{fd}\_min = -7.3$; Transmission Line: $x_{tE} = 0.1$; $x_{BV} = 0.6$;

UPFC: x_E=0.1; x_B=0.1; K=1; T=0.05; C_{dc}=3; V_{dc}=2;

APPENDIX B

The reactance's of equations (5)-(10) are:

$$X_{qE} = X_q + X_{tE}\,, X_{dE} = X'_d + X_{tE}\,, \quad X_{BB} = X_B + X_{BV}$$

$$X_{d1} = X_E(1+\frac{(X_{tE}+X'_d)(X_E+X_T)}{X_E X_T})\,, X_{d2} = X_{BB}X_{d1} + X_E X_{dE}\,, \qquad X_{d3} = \frac{1}{X_{d2}}(\frac{X_E X_{dE}}{X_T} - X_{d1})\,,$$

$$X_{d4} = \frac{1}{X_{d2}}(X_{d1} - X_E - \frac{X_E X_{dE}}{X_T})\,,$$

$$X_{d5} = \frac{1}{X_E}(1+X_{BB}X_{d3})\,, X_{d7} = \frac{1}{X_E}(1-X_{BB}\frac{X_{d1}}{X_{d2}})\,, X_{q1} = X_E(1+\frac{(X_{tE}+X_q)(X_E+X_T)}{X_E X_T})\,, X_{q2} = X_{BB}X_{q1} + X_E X_{qE}\,,$$

$$X_{q3} = \frac{1}{X_{q2}}(-\frac{X_E X_{qE}}{X_T} + X_{q1})\,, X_{q4} = \frac{1}{X_{q2}}(-X_{q1} + X_E + \frac{X_E X_{qE}}{X_T}) \; X_{q5} = \frac{1}{X_E}(-1+X_{BB}X_{q3})\,,$$

$$X_{q6} = \frac{1}{X_E}(1+X_{BB}X_{q4}) \qquad X_{q7} = \frac{1}{X_E}(-1+X_{BB}\frac{X_{q1}}{X_{q2}})$$

APPENDIX C

Numerical value of matrices A and B, and initial value of power system currents and voltages are given in Tables 8-11.

a) Nominal Loading

Table 8. Numerical value of matrices A and B, and initial value of power system currents and voltages in nominal loading condition

$$A=\begin{bmatrix} 0 & 377 & 0 & 0 & 0 \\ -0.0168 & 0 & -0.1696 & 0 & -0.0245 \\ -0.0393 & 0 & -0.484 & 0.1983 & 0.1099 \\ 58.80 & 0 & -333.70 & -20.00 & -304.59 \\ -0.2613 & 0 & 0.2684 & 0 & -0.0394 \end{bmatrix} \qquad B=\begin{bmatrix} 0 & 0 & 0 & 0 & 0 \\ 0 & -0.046 & 0.17 & 0.0119 & 0.001 \\ 0 & 0.201 & 0.1501 & 0.019 & -0.0011 \\ -1000 & -561.2 & 0.60 & -20.8 & -4.80 \\ 0 & -0.10 & -0.60 & 0.20 & -0.0073 \end{bmatrix}$$

V_t (pu)	i_t (pu)	E_q' (pu)	V_{Et} (pu)	i_{SE} (pu)
0.5033+j0.9009	0.4853+j08389	j1.0465	0.5872+j0.8524	0.4331+j0.2882
i_{SH} (pu)	i_{TL} (pu)	V_b (pu)	V_{SE} (pu)	V_{SH} (pu)
-0.382+j0.2657	0.4341+j0.2849	0.95+j0.288	-0.0534+j0.0879	0.6138+j0.8906

b) Light Loading

Table 9. Numerical value of matrices A and B, and initial value of power system currents and voltages in light loading condition

$$A=\begin{bmatrix} 0 & 377 & 0 & 0 & 0 \\ -0.0232 & 0 & -0.0575 & 0 & -0.0041 \\ -0.0172 & 0 & -0.484 & 0.1983 & 0.1251 \\ 20.2297 & 0 & -376.98 & -20.00 & -277.073 \\ -0.359 & 0 & 0.084 & 0 & -0.0140 \end{bmatrix} \qquad B=\begin{bmatrix} 0 & 0 & 0 & 0 & 0 \\ 0 & -0.0088 & 0.20 & 0.0065 & -0.0019 \\ 0 & 0.24 & 0.048 & -0.017 & -0.0023 \\ -1000 & -5327 & 7.60 & 43.70 & 3.60 \\ 0 & -0.049 & -0.60 & 0.0293 & -0.0294 \end{bmatrix}$$

V_t (pu)	i_t (pu)	E_q' (pu)	V_{Et} (pu)	i_{SE} (pu)
0.1706+j1.0178	0.0624+j0.2843	j1.0365	0.199+j1.0116	0.2184+j0.1053
i_{SH} (pu)	i_{TL} (pu)	V_b (pu)	V_{SE} (pu)	V_{SH} (pu)
-0.2358+j0.0096	0.0797+j0.1693	0.4191+0.907	-0.1043+j0.1366	0.20+j1.0351

c) Heavy Loading

TABLE 10. NUMERICAL VALUE OF MATRICES A AND B, AND INITIAL VALUE OF POWER SYSTEM CURRENTS AND VOLTAGES IN HEAVY LOADING CONDITION

$$A=\begin{bmatrix} 0 & 377 & 0 & 0 & 0 \\ -0.0157 & 0 & -0.157 & 0 & -0.0309 \\ -0.040 & 0 & -0.484 & 0.1983 & 0.1051 \\ 66.1087 & 0 & -341.103 & -20.00 & -283.61 \\ -0.2242 & 0 & 0.2418 & 0 & -0.0339 \end{bmatrix} \qquad B=\begin{bmatrix} 0 & 0 & 0 & 0 & 0 \\ 0 & -0.10 & 0.20 & 0.0112 & 0.0015 \\ 0 & 0.20 & 0.10 & 0.02 & -0.0009 \\ -1000 & -566.6 & -10.1 & -28.9 & 4.5 \\ 0 & -0.10 & -0.60 & 0.20 & -0.007 \end{bmatrix}$$

V_t (pu)	i_t (pu)	E_q' (pu)	V_{Et} (pu)	i_{SE} (pu)
0.4657+j0.9209	0.8269+j0.7762	j1.169	0.5434+j0.8382	0.4675+j0.3531
i_{SH} (pu)	i_{TL} (pu)	V_b (pu)	V_{SE} (pu)	V_{SH} (pu)
-0.113+j0.0915	0.4724+j0.3317	0.974+j0.224	-0.0428+j0.099	0.5525+j0.8495

d) Leading power factor loading

Table 11. Numerical value of matrices A and B, and initial value of power system currents and voltages in leading power factor loading condition

$$A=\begin{bmatrix} 0 & 377 & 0 & 0 & 0 \\ -0.0188 & 0 & -0.1491 & 0 & -0.0105 \\ -0.0343 & 0 & -0.484 & 0.1983 & 0.1212 \\ 41.1163 & 0 & -345.33 & -20.00 & -311.8537 \\ -0.3236 & 0 & 0.2364 & 0 & -0.0383 \end{bmatrix} \qquad B=\begin{bmatrix} 0 & 0 & 0 & 0 & 0 \\ 0 & -0.198 & 0.20 & 0.0112 & 0.0015 \\ 0 & 0.20 & 0.10 & 0.0048 & -0.0022 \\ -1000 & -563.9 & 16.30 & 15.40 & 5.1 \\ 0 & -0.10 & -0.60 & 0.10 & -0.0144 \end{bmatrix}$$

V_t (pu)	i_t (pu)	E_q' (pu)	V_{Et} (pu)	i_{SE} (pu)
0.4425+j0.9323	0.0282+j0.7374	j0.9408	0.5162+j0.9295	0.3243+j0.1965
i_{SH} (pu)	i_{TL} (pu)	V_b (pu)	V_{SE} (pu)	V_{SH} (pu)
-0.5881+j0.2955	0.292+j0.2454	0.835+j0.549	-0.1029+j0.0230	0.5458+j0.9883